Electronic Supplementary Material (ESI) for Journal of Materials Chemistry A.

Operando synchrotron X-ray studies of MnVOH@SWCNT nanocomposites as cathodes for high-performance aqueous zinc-ion batteries

Sanna Gull, Shao-Chu Huang, Chung-Sheng Ni, Shih-Fu Liu, Wei-Hsiang Lin, Han-Yi Chen*
Department of Materials Science and Engineering, National Tsing Hua University, 101, Sec. 2, Kuang-Fu Road, Hsinchu 30013, Taiwan

* Corresponding author: Prof. Han-Yi Chen (hanyi.chen@mx.nthu.edu.tw)

Table S1. Comparison of various cathodes in aqueous zinc-ion batteries.

Cathode	Anode	Electrolyte	Potential window / V	Specific capacity	Cycling performance	Ref.
$Al_{0.84}V_{12}O_{30.3}\cdot nH_2O$	Zn foil	3 M $Zn(CF_3SO_3)_2$	0.2 1.6	380 mA h g^{-1} at 0.05 A g^{-1}	107% capacity retention after 3000 cycles at 4 A g^{-1}	[S1]
$Mg_{0.34}V_2O_5\cdot nH_2O$	Zn foil	3 M $Zn(CF_3SO_3)_2$	0.2 1.8	352 mA h g^{-1} at 100 mA g^{-1}	97% capacity retention after 2000 cycles at 5 A g^{-1}	[S2]
$Zn_{0.25}V_2O_5\cdot nH_2O$	Zn foil	1 M $ZnSO_4$	0.5 1.4	300 mA h g^{-1} at 50 mA g^{-1}	80% capacity retention after 1000 cycles at 2.4 A g^{-1}	[S3]
$CaV_6O_{16}\cdot 3H_2O$	Zn foil	3 M $Zn(CF_3SO_3)_2$	0.2 1.6	367 mA h g^{-1} at 50 mA g^{-1}	100% capacity retention after 300 cycles at 0.5 A g^{-1}	[S4]
V_2O_5/CNT	Zn foil	1 M $ZnSO_4$	0.2 1.7	312 mA h g^{-1} at 1000 mA g^{-1}	81% capacity retention after 2000 cycles at 1 A g^{-1}	[S5]
VO_2 /Graphene	Zn foil	3 M $Zn(CF_3SO_3)_2$	0.3 1.3	276 mA h g^{-1} at 1000 mA g^{-1}	99% capacity retention after 1000 cycles at 4 A g^{-1}	[S6]
$Zn_3[Fe(CN)_6]_2$	Zn foil	3 M $ZnSO_4$	0.8 1.9	66 mA h g^{-1} at 60 mA g^{-1}	81% capacity retention after 200 cycles at 0.3 A g^{-1}	[S7]
Polyaniline	Zn foil	1 M $Zn(CF_3SO_3)_2$	0.5 1.5	95 mA h g^{-1} at 5000 mA g^{-1}	92% capacity retention after 3000 cycles at 5 A g^{-1}	[S8]
γ-MnO_2	Zn foil	1 M $ZnSO_4$	1.0 1.8	285 mA h g^{-1} at 0.05 mA cm^{-2}	63% capacity retention after 40 cycles at 0.05 mA cm^{-2}	[S9]
poly(Li_2S_6-random-(1,3-diisopropenylbenzene)) (poly(Li_2S_6-r-DIB) copolymer	Zn foil	1 M $Zn(TFSI)_2$ + 21 M LiTFSI	0.1 2.4	400 mA h g^{-1} at 1000 mA g^{-1}	50% capacity retention over 1600 cycles at 1 A g^{-1}	[S10]
Se/CMK-3	Zn foil	1 M $Zn(TFSI)_2$	0.0 2.2	398 mA h g^{-1} at 1000 mA g^{-1}	81.2% capacity retention after 500 cycles at 1 A g^{-1}	[S11]
5 wt% SWCNT	Zn foil	3 M $Zn(CF_3SO_3)_2$	0.2 1.6	381 mA h g^{-1} at 1000 mA g^{-1}	89% capacity retention after300 cycles at 5 A g^{-1}	This work

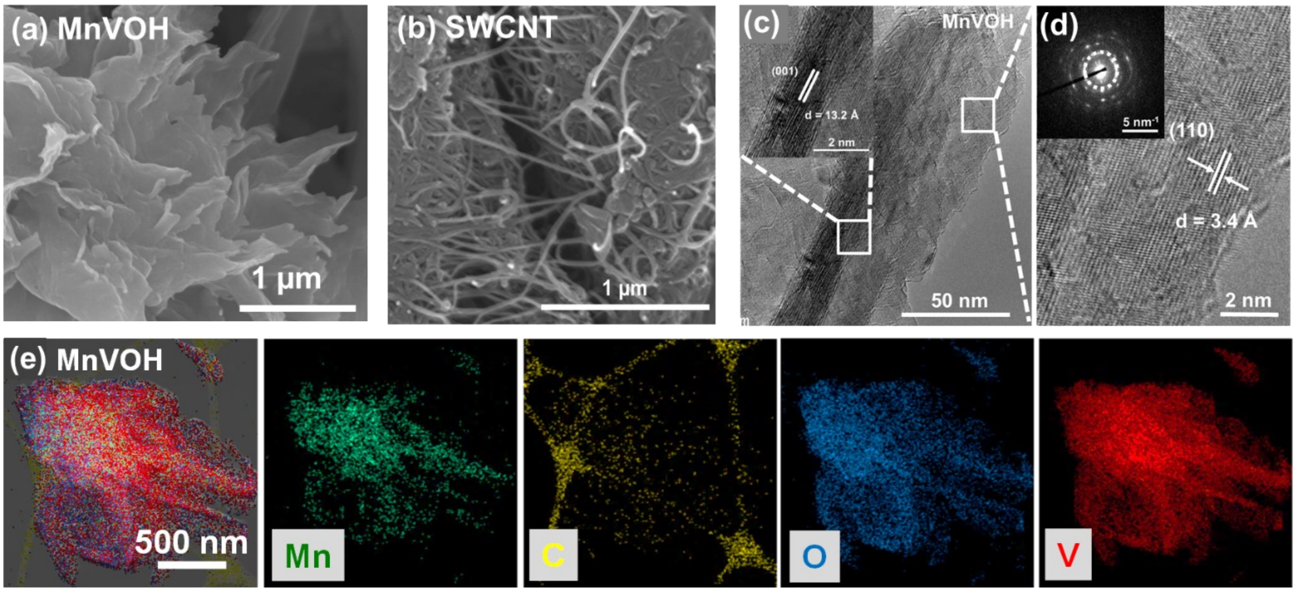

Figure S1. FESEM image of (a) MnVOH, and (b) SWCNT. HRTEM images of MnVOH with: (c) 13.2 Å interlayer spacing; (d) 3.4 Å interlayer spacing (inset is SAED pattern). (e) TEM-EDX mapping images of MnVOH.

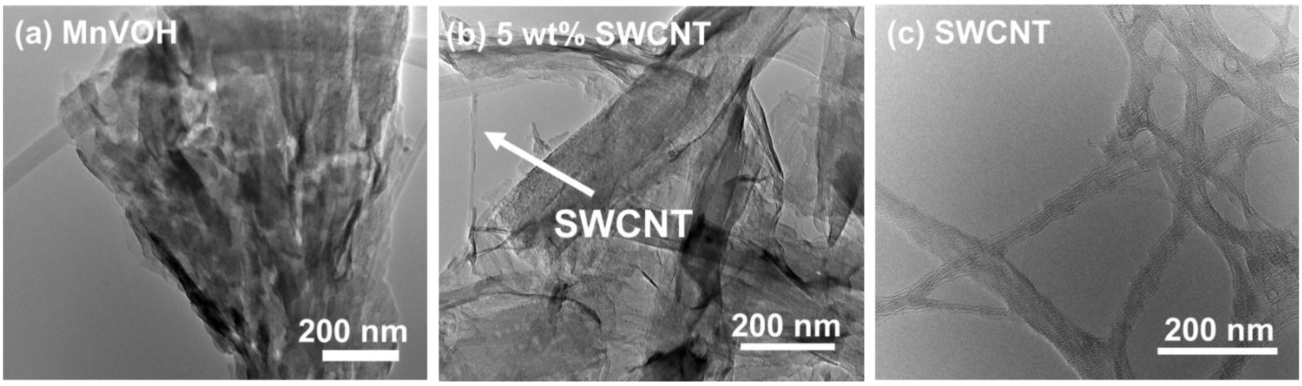

Figure S2. HRTEM images: (a) MnVOH; (b) 5 wt% SWCNT; (c) SWCNT.

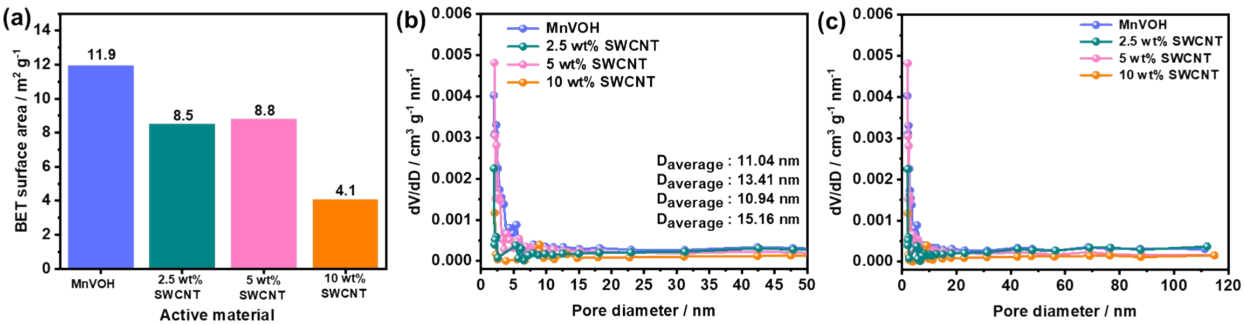

Figure S3. (a) Surface area, (b) pore size distribution curves, and (c) pore size distribution smaller than mesopores for MnVOH, 2.5 wt% SWCNT, 5 wt% SWCNT, and 10 wt% SWCNT.

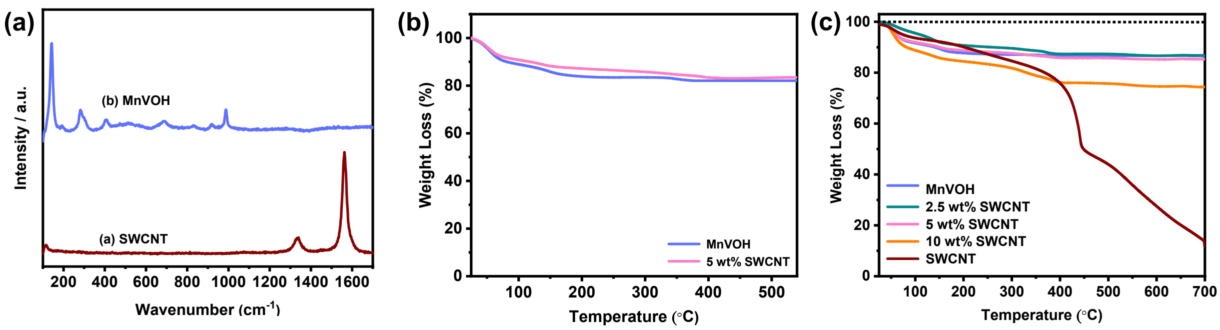

Figure S4. (a) Raman spectrum of SWCNT and MnVOH. (b) TGA curves collected over a temperature range of 25–550 °C for MnVOH and 5 wt% SWCNT in Ar atmosphere. (c) TGA curves collected over a temperature range of 25–700 °C for SWCNT, MnVOH, 2.5 wt% SWCNT, 5 wt% SWCNT, and 10 wt% SWCNT in air atmosphere.

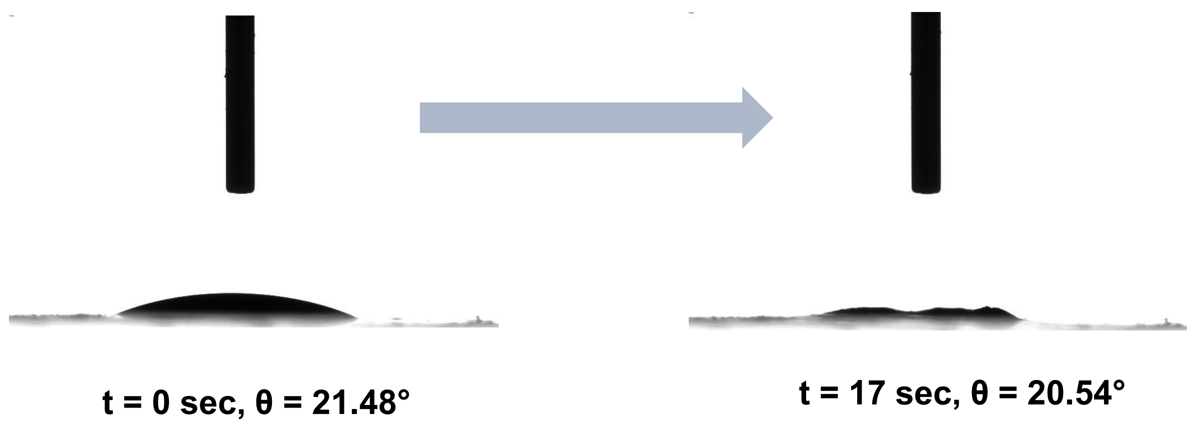

Figure S5. Contact angle measurement of the 5 wt% SWCNT nanocomposite material.

Table S2. Weight percentage of the SWCNT in three MnVOH@SWCNT nanohybrids in precursors and final products.

Form	Weight percentage (wt%)		
Precursors	2.5	5	10
Final products	0.3	2.4	18.2

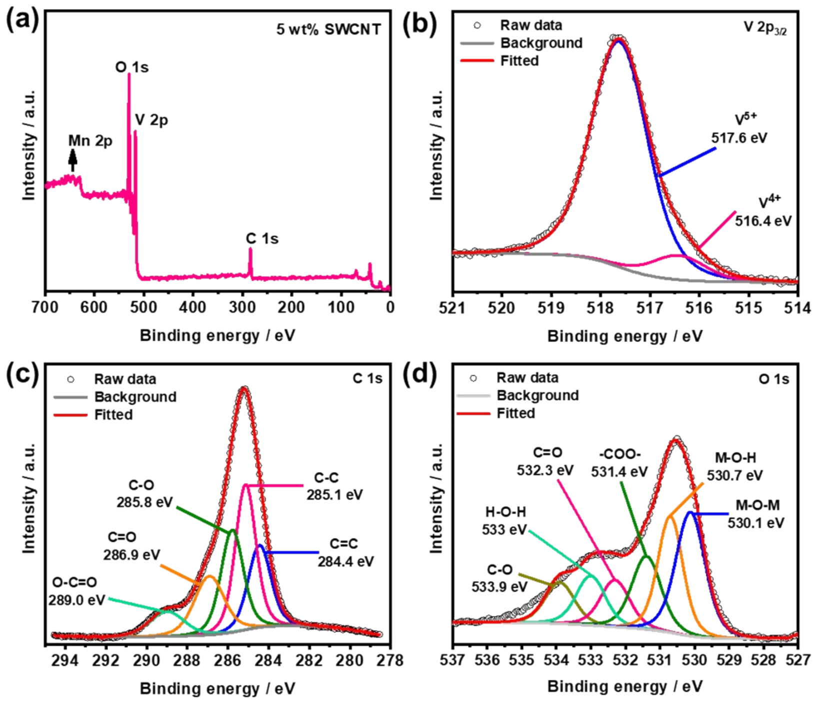

Figure S6. XPS wide spectrum of 5 wt% SWCNT: (a) Survey, (b) V $2p_{3/2}$, and (c) C 1s and (d) O 1s.

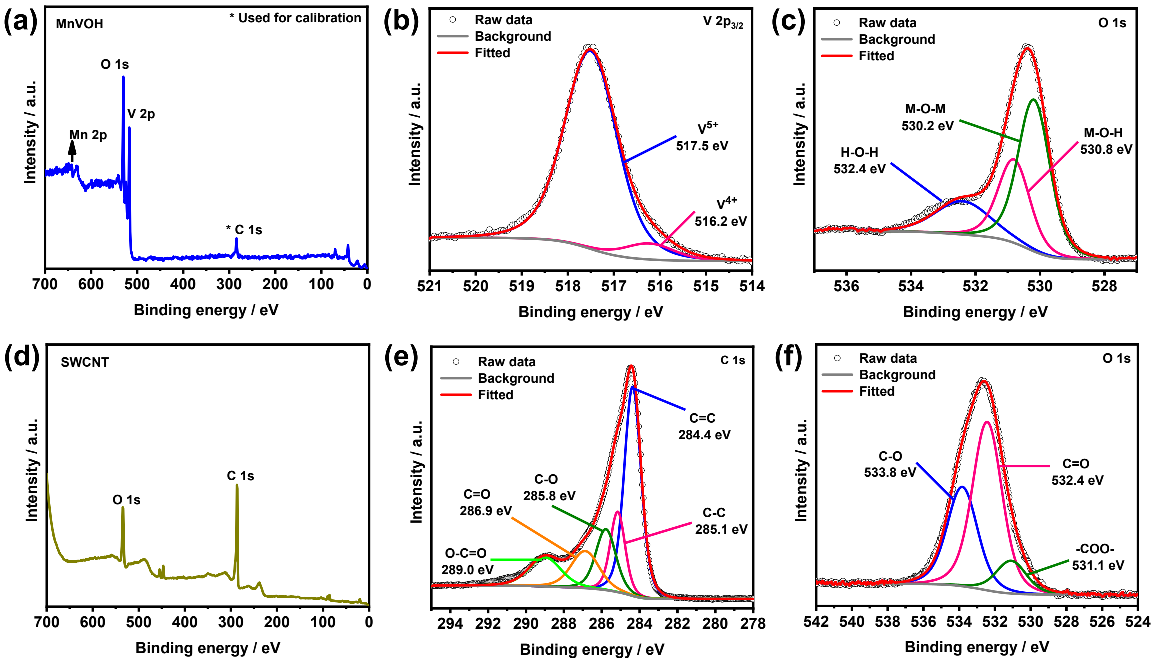

Figure S7. XPS spectrum of MnVOH: (a) Survey, (b) V $2p_{3/2}$, and (c) O 1s; XPS spectrum of SWCNT (d) Survey, (e) C 1s, and (f) O 1s.

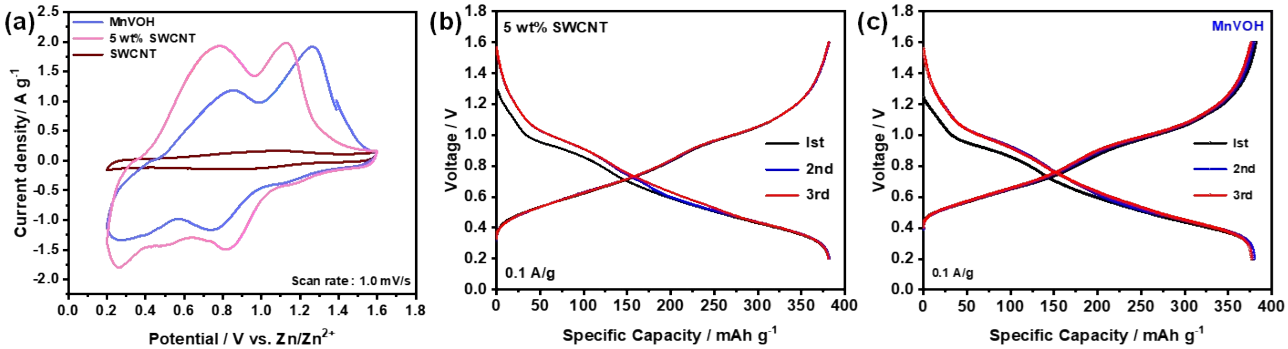

Figure S8. Electrochemical performance: (a) Cyclic voltammetry of MnVOH, 5 wt% SWCNT, and SWCNT at a scan rate of 1.0 mV s^{-1}. GCD curves of (b) 5 wt% SWCNT, and (c) MnVOH at a current density at 0.1 A g^{-1}.

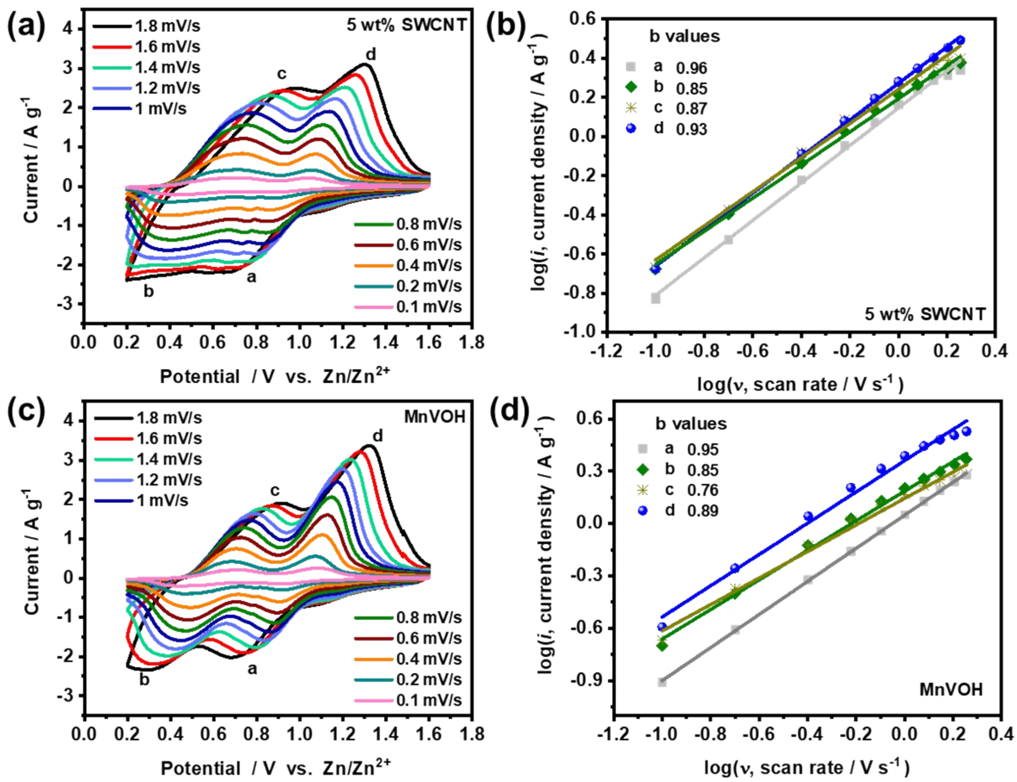

Figure S9. CV curves collected at different scan rates (0.1–1.8 mV s^{-1}) for (a) 5 wt% SWCNT , (c) MnVOH. Determination of the b-value at intercalation and deintercalation peaks of five peaks obtained in the CV curves for (b) 5 wt% SWCNT, (d) MnVOH.

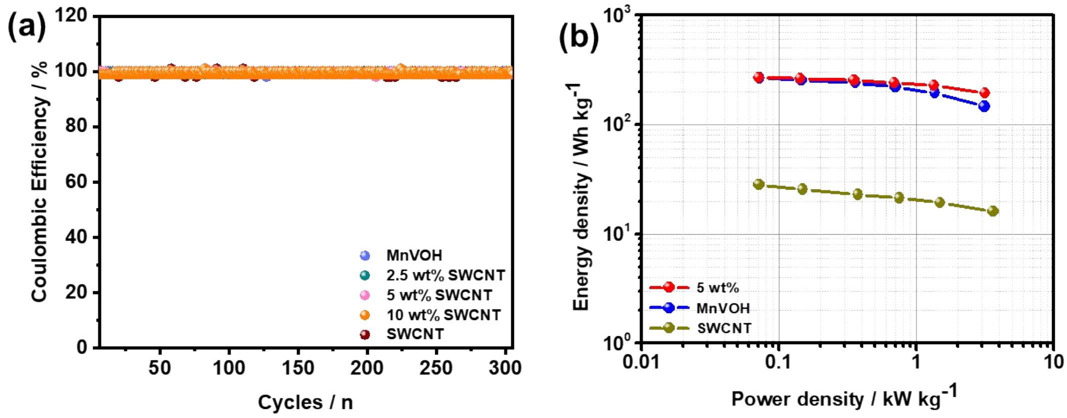

Figure S10. (a) Coulombic efficiency vs. cycles for MnVOH, 2.5 wt% SWCNT, 5 wt% SWCNT, and 10 wt% SWCNT. (b) Ragone plots of SWCNT, MnVOH, and 5 wt% SWCNT.

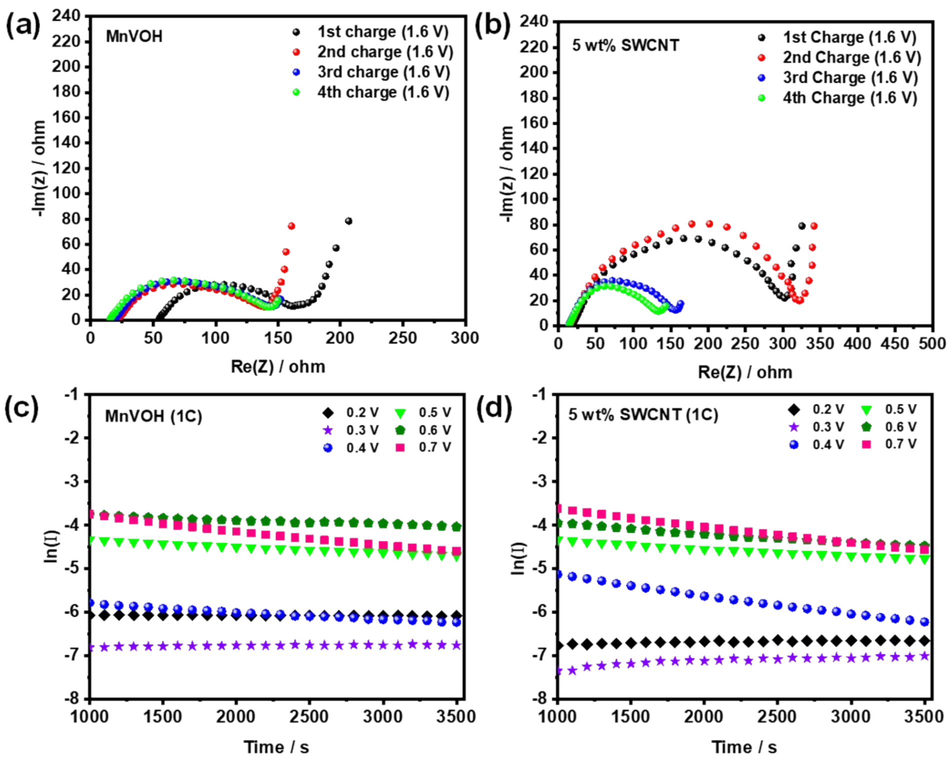

Figure S11. (a–b) Nyquist plots at fully charged state during 1st, 2nd, 3rd, and 4th cycles; (c–d) ln(I) vs. time of chronoamperometry.

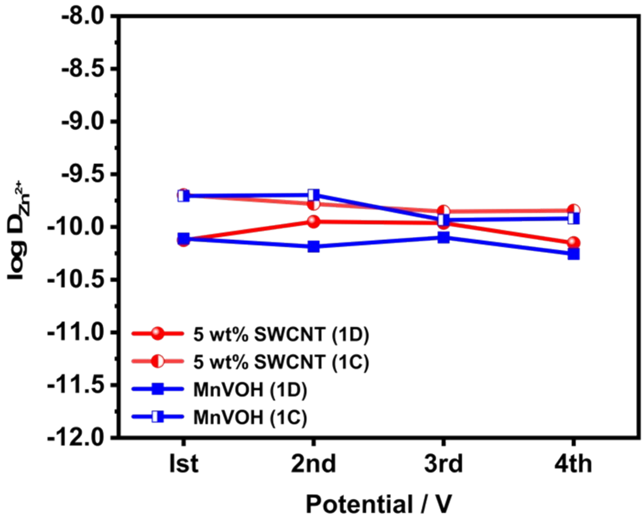

Figure S12. Comparison of the diffusion coefficient of the 5 wt% SWCNT and MnVOH electrodes measured using EIS method.

Table S3. Zn^{2+} Diffusion Coefficient of ZIB Cathode Materials.

Material	**Zn^{2+} diffusion coefficient ($cm^2\ s^{-1}$)**	**Method**	**Ref.**
$V_2O_5.nH_2O$/Graphene	6.0×10^{-13}	EIS	[S12]
MnVO	3.2×10^{-12}	EIS	[S13]
$V_2O_5{\cdot}nH_2O$	3.3×10^{-13}	GITT	[S14]
$Mg_{0.14}V_2O_{5+\delta}{\cdot}nH_2O$	2.0×10^{-13}	GITT	[S14]
$Cu_{0.15}V_2O_{5+\delta}{\cdot}nH_2O$	1.6×10^{-12}	GITT	[S1]
$Al_{0.84}V_{12}O_{30.3}{\cdot}nH_2O$	5.6×10^{-13}	EIS	[S1]
$KV_{12}O_{30-y}{\cdot}nH_2O$	6.6×10^{-14}	EIS	[S15]
5 wt% SWCNT	2.0×10^{-11}	PITT	**This work**
5 wt% SWCNT	5.1×10^{-10}	EIS	**This work**

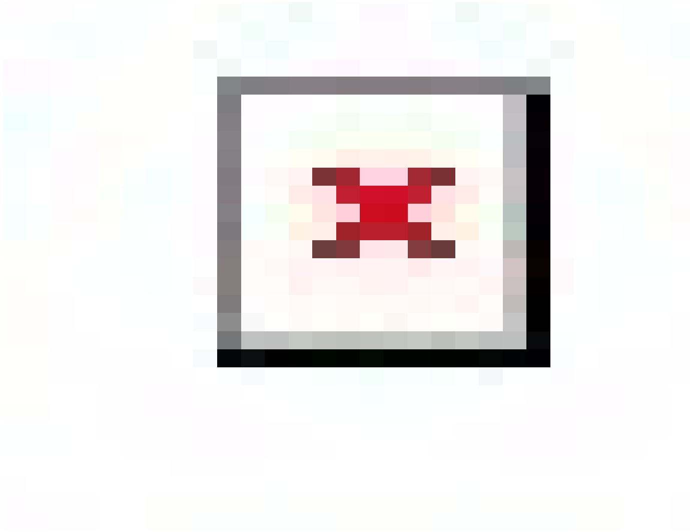

Figure S13. Normalized synchrotron V K-edge XANES spectra of MnVOH and 5 wt% SWCNT.

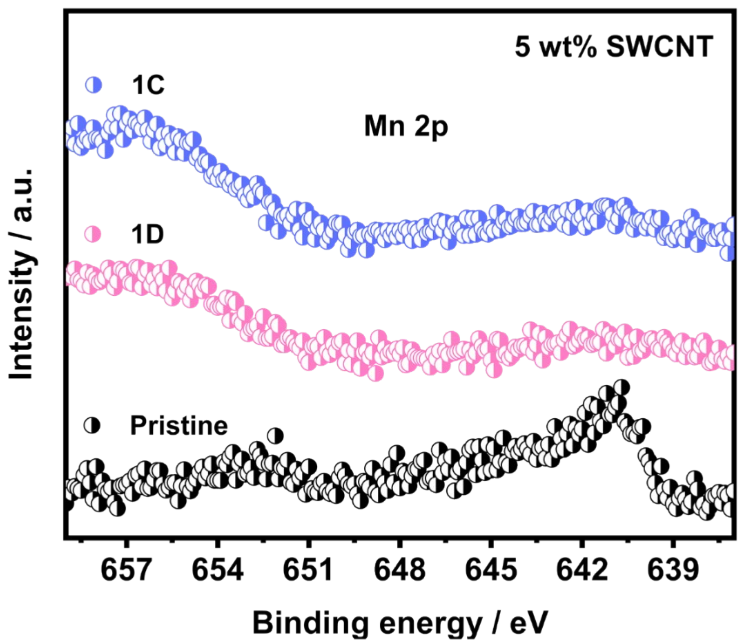

Figure S14. Ex-situ XPS of Mn 2p in the pristine, discharge to 0.2 V, and charge to 1.6 V states in the first cycle.

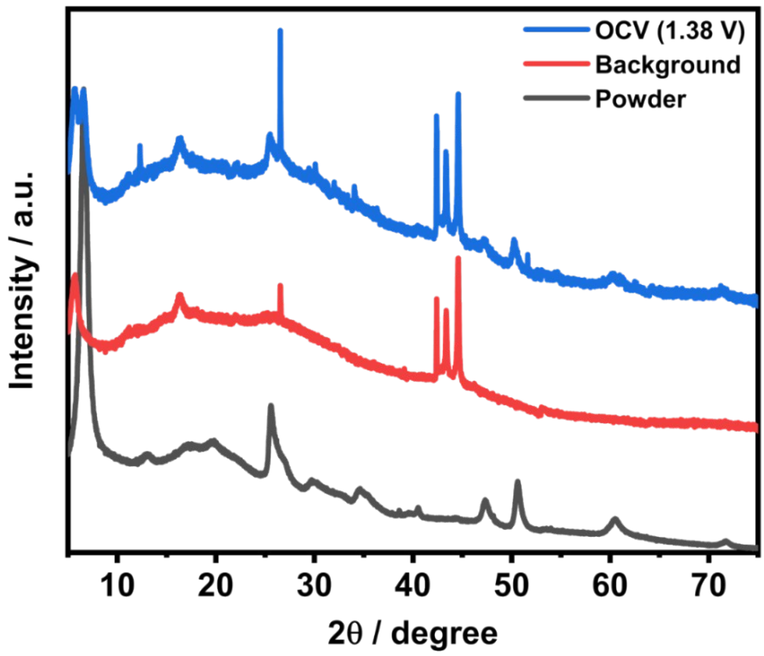

Figure S15. XRD patterns of pristine powder, background, and OCV for *operando* XRD measurement.

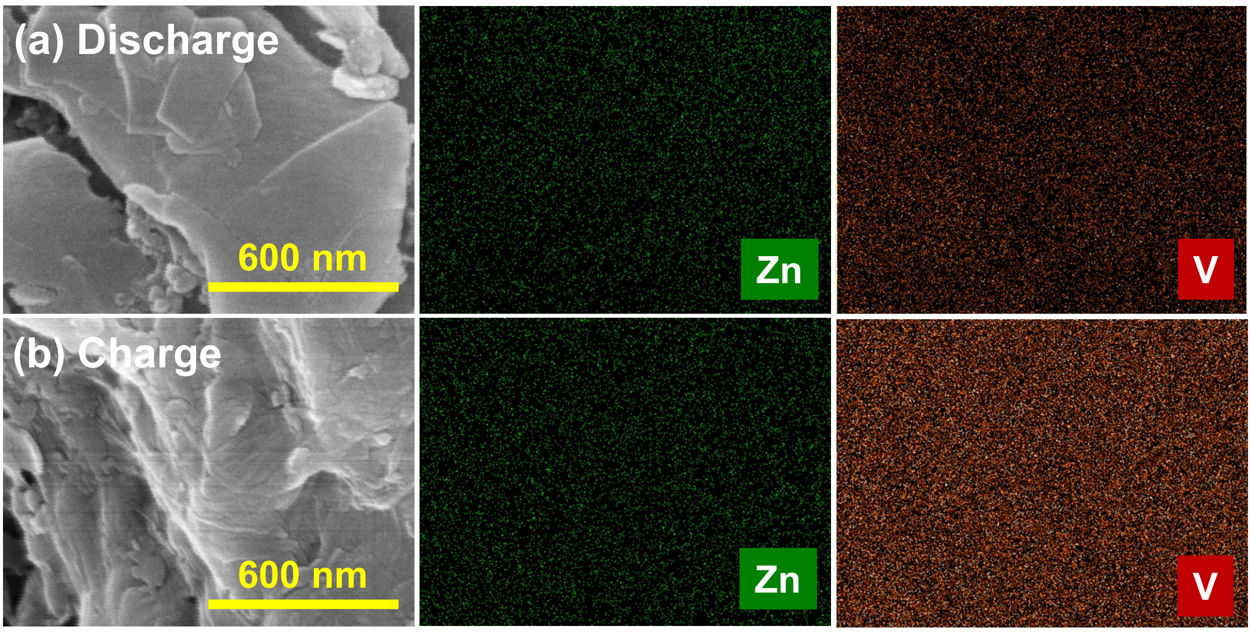

Figure S16. SEM images and the corresponding EDS mapping images of fully discharged (a) and charged (b) electrode materials of MnVOH@SWCNT (5 wt% SWCNT).

References:

[S1] J. Zheng, C. Liu, M. Tian, X. Jia, E. P. Jahrman, G. T. Seidler, S. Zhang, Y. Liu, Y. Zhang, C. Meng and G. Cao, *Nano Energy*, 2020, **70**, 104519.

[S2] F. Ming, H. Liang, Y. Lei, S. Kandambeth, M. Eddaoudi and H. N. Alshareef, *ACS Energy Lett.*, 2018, **3**, 2602–2609.

[S3] D. Kundu, B. D. Adams, V. Duffort, S. H. Vajargah and L. F. Nazar, *Nat. Energy*, , DOI:10.1038/nenergy.2016.119.

[S4] X. Liu, H. Zhang, D. Geiger, J. Han, A. Varzi, U. Kaiser, A. Moretti and S. Passerini, *Chem. Commun.*, 2019, **55**, 2265–2268.

[S5] B. Yin, S. Zhang, K. Ke, T. Xiong, Y. Wang, B. K. D. Lim, W. S. V. Lee, Z. Wang and J. Xue, *Nanoscale*, 2019, **11**, 19723–19728.

[S6] X. Dai, F. Wan, L. Zhang, H. Cao and Z. Niu, *Energy Storage Mater.*, 2019, **17**, 143–150.

[S7] L. Zhang, L. Chen, X. Zhou and Z. Liu, *Sci. Rep.*, 2015, **5**, 1–11.

[S8] F. Wan, L. Zhang, X. Wang, S. Bi, Z. Niu and J. Chen, *Adv. Funct. Mater.*, 2018, **28**, 1–8.

[S9] M. H. Alfaruqi, V. Mathew, J. Gim, S. Kim, J. Song, J. P. Baboo, S. H. Choi and J. Kim, *Chem. Mater.*, 2015, **27**, 3609–3620.

[S10] Y. Zhao, D. Wang, X. Li, Q. Yang, Y. Guo, F. Mo, Q. Li, C. Peng, H. Li and C. Zhi, *Adv. Mater.*, 2020, **32**, 1–10.

[S11] Z. Chen, F. Mo, T. Wang, Q. Yang, Z. Huang, D. Wang, G. Liang, A. Chen, Q. Li, Y. Guo, X. Li, J. Fan and C. Zhi, *Energy Environ. Sci.*, 2021, **14**, 2441–2450.

[S12] M. Yan, P. He, Y. Chen, S. Wang, Q. Wei, K. Zhao, X. Xu, Q. An, Y. Shuang, Y. Shao, K. T. Mueller, L. Mai, J. Liu and J. Yang, *Adv. Mater.*, 2018, **30**, 1–6.

[S13] C. Liu, Z. Neale, J. Zheng, X. Jia, J. Huang, M. Yan, M. Tian, M. Wang, J. Yang and G. Cao, *Energy Environ. Sci.*, 2019, **12**, 2273–2285.

[S14] C. Liu, M. Tian, M. Wang, J. Zheng, S. Wang, M. Yan, Z. Wang, Z. Yin, J. Yang and G. Cao, *J. Mater. Chem. A*, 2020, **8**, 7713–7723.

[15] M. Tian, C. Liu, J. Zheng, X. Jia, E. P. Jahrman, G. T. Seidler, D. Long, M. Atif, M. Alsalhi and G. Cao, *Energy Storage Mater.*, 2020, **29**, 9–16.